Korean J. Chem. Eng., 36(12), 2118-2124 (2019)
DOI: 10.1007/s11814-019-0401-0

pISSN: 0256-1115
eISSN: 1975-7220

Controlling the recombination of electron-hole pairs by changing the shape of ZnO nanorods via sol-gel method using water and their enhanced photocatalytic properties

Yong Sik Seo and Seong-Geun Oh[†]

Department of Chemical Engineering, Hanyang University, Seoul 04761, Korea

(*Received 30 July 2019 • accepted 8 October 2019*)

Abstract−ZnO nanorods were prepared through a sol-gel process by adding various amounts of water at low temperature and atmospheric pressure conditions for application as a photocatalyst. The 1-D ZnO nanostructures can overcome fast recombination of photogenerated electrons and holes that inhibits photocatalytic efficiency. X-ray diffractometer and transmission electron microscopy measurements confirmed that the (002)/(100) intensity ratio increased from 0.83 to 1.34 and the morphology of the ZnO nanoparticles was changed from a spherical shape to nanorods with the addition of water. UV-vis spectroscopy showed a red shift from 360 nm to 371 nm, which indicates a decrease of the band gap energy. PL measurements of the ZnO nanorods showed a 10^3 times improvement of the NBE/DLE intensity ratio compared to the ZnO nanospheres. When the photocatalytic efficiency of the ZnO nanoparticles was estimated for the degradation of methylene blue dye under irradiation of UV light, the photocatalytic kinetic constant increased from 0.067 min^{-1} to 0.481 min^{-1}. As a result, longer ZnO nanorods showed better photocatalytic performance.

Keywords: ZnO, Sol-gel Process, Nanorods, Photocatalyst, Electron-hole Recombination

INTRODUCTION

Semiconductor photocatalysts have been attracting significant attention owing to their excellent ability to degrade harmful organic pollutants [1,2]. The most extensively studied semiconductor photocatalysts are TiO_2 [3], ZnO [4], and CdS [5,6] because of their band gap energy resulting from their electronic structure [7]. Among these materials, ZnO is most widely used due to its non-toxicity, abundance, and high electron mobility [8-10]. However, the lifetime of ZnO photocatalysts is shortened as a result of fast recombination of electrons and holes, which causes deterioration of the photocatalytic efficiency [11]. It was suggested that morphology control of ZnO can overcome the drawback of fast recombination [12]. One-dimensional (1-D) ZnO nanostructures, including nanorods and nanowires, have been extensively studied for photocatalysts because they promote charge separation by an internal electric field to delocalize electrons, resulting in improved photocatalytic efficiency [13-15]. Various techniques such as hydrothermal evaporation [16], vapor-liquid-solid (VLS) [17], metal-organic chemical vapor deposition (CVD) [18], electrochemical deposition (ED) [19], molecular beam epitaxy (MBE) [20], and template-based methods [21] have been utilized to synthesize 1-D ZnO nanostructures. These methods require high temperature and pressure conditions, which limit large-scale production and yield high defect products with poor purity [22,23]. Thus, there is a need for a facile synthetic method for 1-D ZnO nanostructures at low temperature and atmospheric pressure conditions.

The synthesis of 1-D ZnO nanostructures at low temperatures includes a sonochemical route [24], aqueous alcohol solution [25, 26], and surfactant-assisted growth [27]. These methods have been used for relatively large-scale production and low defect products with good purity. However, at low temperatures these synthetic methods have complex multi-step problems in the manufacturing process. Therefore, morphological change via an uncomplicated synthetic method of 1-D ZnO nanostructures is highly needed.

Many previous studies reported changing the morphology of zinc oxide by adding surfactants or heating treatment. In this study, the one-dimensional zinc oxide nanorods by adding water were prepared in one-pot after the formation of zinc oxide nanoparticles during the sol-gel process. This process is simple and it is easy to control the growth of zinc oxide because all of the reactions are completed in one reactor and at a low temperature. In the synthetic method of 1-D ZnO nanostructures, it has been demonstrated that water can induce fast hydrolysis of the zinc precursor and affect the nucleation process of ZnO [28]. The hydrolysis after adding water is closely related to the shape and size of the ZnO nanomaterials. During the hydrolysis, Zn-rich and O-rich surfaces are generated as the nanoparticles regrow, which creates a potential difference between each surface that facilitates charge separation and maximizes the photocatalytic efficiency [29]. The aspect ratios and sizes of ZnO nanorods were investigated as functions of the amount of water added into the reaction medium during the sol-gel process. The photocatalytic efficiency of various ZnO nanorods was also measured.

EXPERIMENTAL

1. Materials

Zinc acetate dehydrate (Zn $(CH_3COO)_2 \cdot 2H_2O$, Sigma-Aldrich), potassium hydroxide (KOH, JUNSEI), and anhydrous ethyl alco-

---

[†] To whom correspondence should be addressed.
E-mail: seongoh@hanyang.ac.kr

hol (ethanol 99.9%, DAEJUNG) were used to prepare the ZnO nanostructures. Methylene blue (MB) dye purchased from DAEJUNG Chemicals in Korea was used as an organic pollutant. The 1-butanol (JUNSEI) was used as the dispersion medium of ZnO particles. 2-(2-methoxyethoxy) acetic acid (MEA) as a dispersing agent was purchased form Sigma-Aldrich, USA. Finally, deionized water (Millipore ICW 3000 system) was used as a morphological changing agent.

2. Preparation of Spherical ZnO Nanoparticles

ZnO was synthesized in ethanol by the sol-gel process utilizing zinc acetate dehydrate ($Zn(CH_3COO)_2{\cdot}2H_2O$, Sigma-Aldrich) and potassium hydroxide (KOH, JUNSEI) [30]. $Zn(CH_3COO)_2{\cdot}2H_2O$ (10 mmol) was dissolved fully in 100 mL of ethanol under stirring at 60 °C for 30 min. When the zinc acetate dehydrate materials were completely dissolved, a transparent solution was obtained. Then, KOH (20 mmol) completely dissolved in 50 mL of ethanol at 60 °C for 30 min was added dropwise into a transparent zinc acetate dehydrate solution. The mixture was stirred at 60 °C for 3 h and held at room temperature for 4 h. The samples were then centrifuged at 3,000 rpm for 15 min twice to obtain precipitates. The precipitates were then dried at 80 °C for 12 h.

3. Morphological Modification of ZnO Nanorods

To synthesize the ZnO nanorods, various amounts of water (1, 3, 5 ml) were added dropwise into the mixture of Zn acetate and the KOH solution after reaction at 60 °C for 3 h [31]. These solutions were stirred at 60 °C for 6 h and held at room temperature for 4 h. The centrifuging and washing steps of this precipitate were the same as those mentioned above. Fig. 1 shows the scheme for the formation of ZnO nanorods by adding water. When water is added, the ZnO nanoparticles grow along the c-axis. The crystal growth velocity of the ZnO nanoparticles is different as $V\ (0001) > V\ (01\bar{1}0) > V\ (000\bar{1})$. Therefore, the ideal shape of ZnO crystals can be considered to be nanorods [32].

4. Characterization

The size and morphology of the ZnO nanostructures (nanosphere or nanorod) were observed using transmission electron microscopy (TEM, JEOL JEM-2100). The ZnO dispersed in 1-butanol was added dropwise on the TEM grid (Carbon Type-B, TED PELLA) and dried in oven at 80 °C for 1 day. An X-ray diffractometer (XRD, Rigaku, D/MAX-2500H) was used to measure the crystal structures of the ZnO powders. The incident wavelength was Cu K-α=0.15406 nm and the detector moved step by step between 25° and 70°. The optical and band gap energies of ZnO nanomaterials were measured using a UV-Vis spectrometer. The photoluminescence spectra (PL spectra, SCINCO, FS-2) were obtained by employing a He-Cd laser (325 nm).

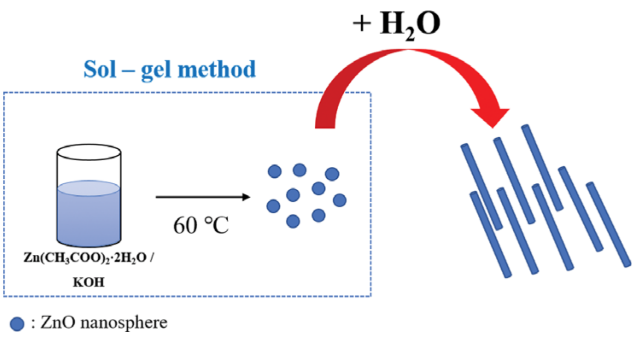

Fig. 1. Schematic representation for the formation of ZnO nanorods by adding water.

5. Photocatalytic Efficiency Evaluation via Methylene Blue Degradation

The photocatalytic efficiency of ZnO nanomaterials was evaluated through the photodegradation of MB under UV light (400 W, UV-H-0.4, Korea). In a typical experiment, the ZnO powders (ZnO nanosphere or ZnO nanorods, 0.05 g) were dispersed in an aqueous MB solution (50 ppm). Before UV light irradiation, the suspensions were sonicated for 30 min and stirred in the dark for 30 min to obtain adsorption-desorption equilibrium. A suspension (7.5 mL) was extracted every two minutes and centrifuged to separate the particles and the supernatant of the MB solution was investigated by a UV-vis spectrophotometer. The highest absorption peak of the aqueous MB solution appeared at a wavelength of 664 nm.

RESULTS AND DISCUSSION

1. Structural Properties and Characterization of ZnO Nanospheres and Nanorods

For convenience, the ZnO nanospheres and nanorods synthesized with different amounts of water (0 ml, 1 mL, 3 mL, and 5 mL of H_2O) are denoted as ZnO NS, ZnO NR1, ZnO NR3, and ZnO NR5, respectively. Fig. 2 shows the XRD patterns of ZnO NS and the ZnO NRs (ZnO NR1, 3, 5), which exhibit similar XRD single peaks, indicating the hexagonal Wurtzite structure of ZnO (JCPDS No. 36-1451). After reaction with the addition of water in the sol-gel method, no specific diffraction peaks were observed in the patterns, which could indicate the complete formation of pure ZnO. Among them, the main 2θ peak intensities at 31.76 and 34.42 degrees are related to the growth of the (100) and (002) planes, respectively. In more detail, Fig. 3 shows a higher (002) peak intensity than the (100) peak intensity. The change of the (002)/(100) intensity

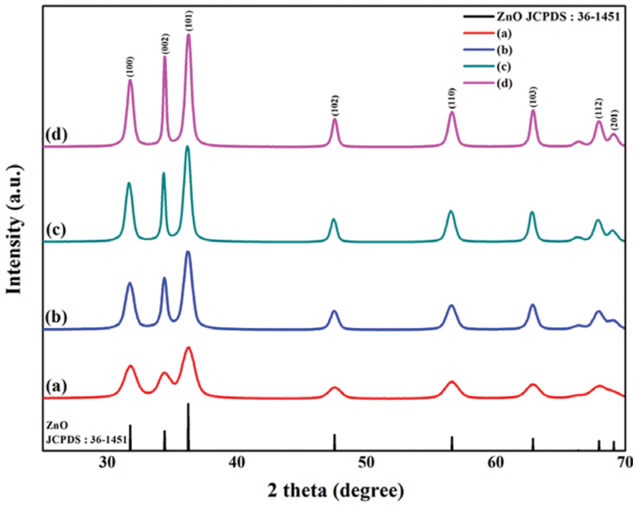

Fig. 2. XRD patterns of the ZnO nanosphere and nanorods with different amount water. (a) ZnO NS, (b) ZnO NR1, (c) ZnO NR3, and (d) ZnO NR5.

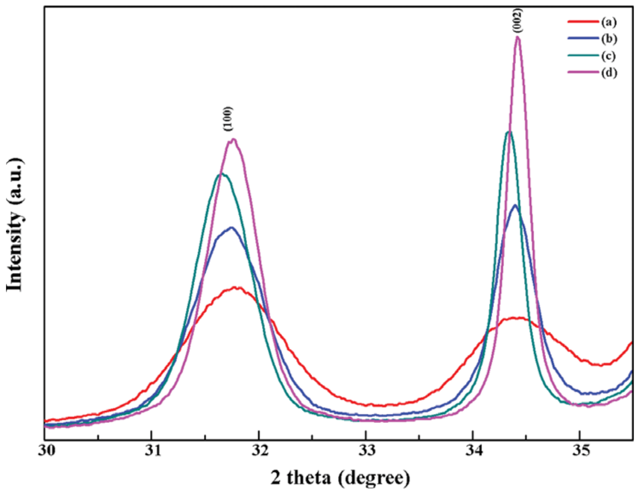

Fig. 3. XRD patterns of the ZnO samples with (100) and (002) peak. (a) ZnO NS, (b) ZnO NR1, (c) ZnO NR3, and (d) ZnO NR5.

Table 1. Intensity details of XRD patterns of the ZnO nanosphere and nanorods. (a) ZnO NS, (b) ZnO NR1, (c) ZnO NR3, and (d) ZnO NR5

Sample	(100) Peak intensity	(002) Peak intensity	Intensity ratio [(002)/(100)]
(a)	34,766	28,786	0.83
(b)	50,046	55,320	1.11
(c)	62,800	72,636	1.16
(d)	70,903	94,970	1.34

Table 2. Aspect ratios through TEM images of the ZnO nanosphere and nanorods prepared with different amounts water

	1 ml	3 ml	5 ml
Diameter (D) (nm)	6.4±1.03	7.4±0.91	7.5±0.62
Length (L) (nm)	13±3.32	48.6±5.1	72.5±6.55
Aspect ratio (L/D)	2.03±0.64	6.57±1.02	9.7±1.05

ratio in the XRD patterns is related to the morphological change from nanospheres to nanorods. A high intensity of the (002) peak (or a large (002)/(100) intensity ratio) indicates the generation of c-axis growth [33,34]. As shown in Table 1, the relative (002)/(100) intensity ratios of the samples were 0.83, 1.11, 1.16, and 1.34. Among them, ZnO NR5 showed a 1.68-times higher ratio than the ZnO NS, which indicates that the c-axis growth of ZnO NS is more dominant than a-axis growth as the amount of water increased. The increases in the ratio of the (002) intensity were 66 and 184 while the (100) ratio increments were 36 and 137, which means that the (002) growth rate is greater than the (100) growth rate. Fig. 4 shows TEM images of the ZnO nanostructures of ZnO NS and ZnO NRs. The images (Figs. 4(b), (c), and (d)) show that the aspect ratio of the nanorods increased as the amount of water increased. The

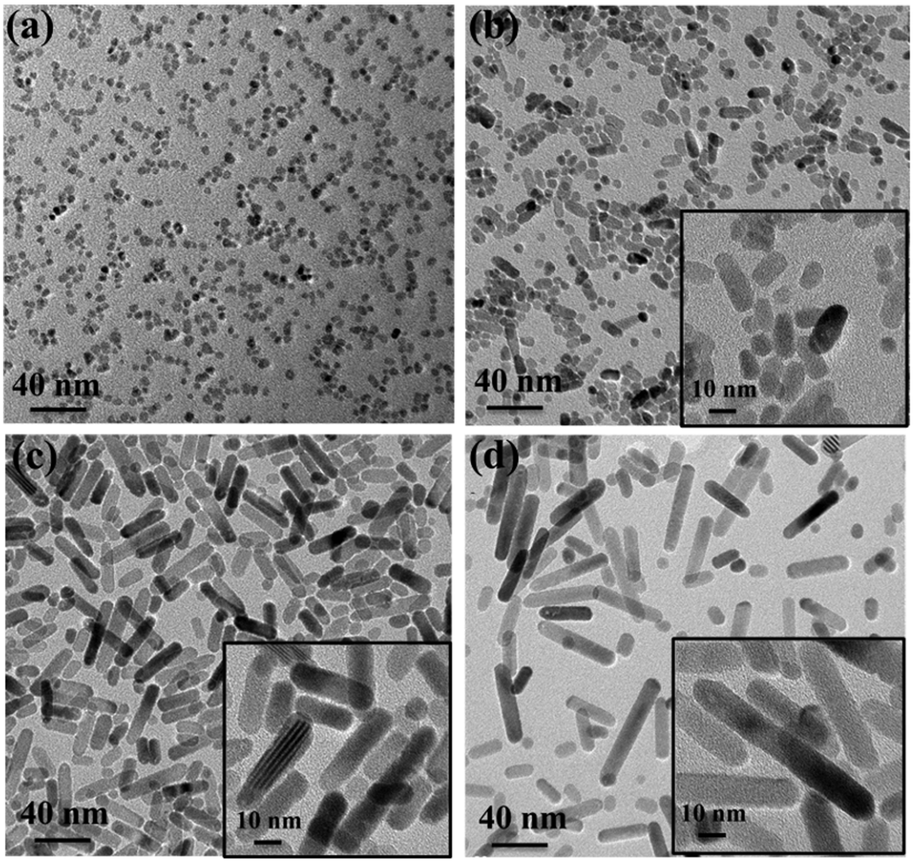

Fig. 4. TEM images of ZnO nanoparticles: (a) ZnO NS, (b) ZnO NR1, (c) ZnO NR3, and (d) ZnO NR5.

lengths of the ZnO NRs were 13, 48.6, and 72.5 nm and the widths were 6.4, 7.4, and 7.5 nm, respectively. In addition, the diameter of the ZnO NS was less than 10 nm. As shown in Table 2, the aspect ratios of the samples are 2, 6.6, and 9.7, respectively. This accretion represents aggregation of ZnO to c-axis growth by the dipole-dipole interplay and van der Waals force between the ZnO nanoparticles [35]. Consequently, morphological changes in the ZnO structures occur due to the addition of water after the sol-gel reaction. The ZnO NRs exhibit an intense 002 XRD peak and large particle size compared to ZnO NS.

2. Optical Properties and Characterization of ZnO Nanostructures

Fig. 5(a) displays the UV-vis absorption peaks of ZnO NS and NRs. A slight red shift of the absorption peak from 360 nm to 371 nm indicates an increase of the nanoparticle size after the addition of water, resulting in an increment of photogenerated electrons and holes on the surface of ZnO due to the internal electric field between the Zn-rich plane (001) and O-rich plane $(00\bar{1})$. This shift also indicates the existence of excess oxygen in the lattice of ZnO NR and the quantum confinement effect [36,37]. Therefore, 1-D ZnO NRs yielded a narrow band gap energy compared to ZnO NS [38]. Fig. 5(B) shows the band gap energies of ZnO NS and NRs (NR1, NR3, NR5), which were calculated to be 3.4 eV, 3.35 eV, 3.33 eV, and 3.32 eV, respectively. These results correspond to the TEM images, which showed an increase of the ZnO nanoparticle size with the addition of water in the sol-gel method. In summary, the larger ZnO nanoparticle size resulted in a red shift and a decrease of the band gap energy by the UV absorption edge.

Fig. 6 exhibits the room temperature photoluminescence (PL) spectra of ZnO NS and ZnO NRs prepared with the addition of different amounts of water. The PL spectra of the samples were gauged using a He-Cd lamp with an excitation wavelength of 325 nm. In Fig. 6(A), all PL spectra show two peaks, which indicates the near band edge (NBE) emission located in the ultraviolet region from 360 nm to 385 nm and the broad deep level (DL) emission located in the visible region around 550 nm [39,40]. The NBE

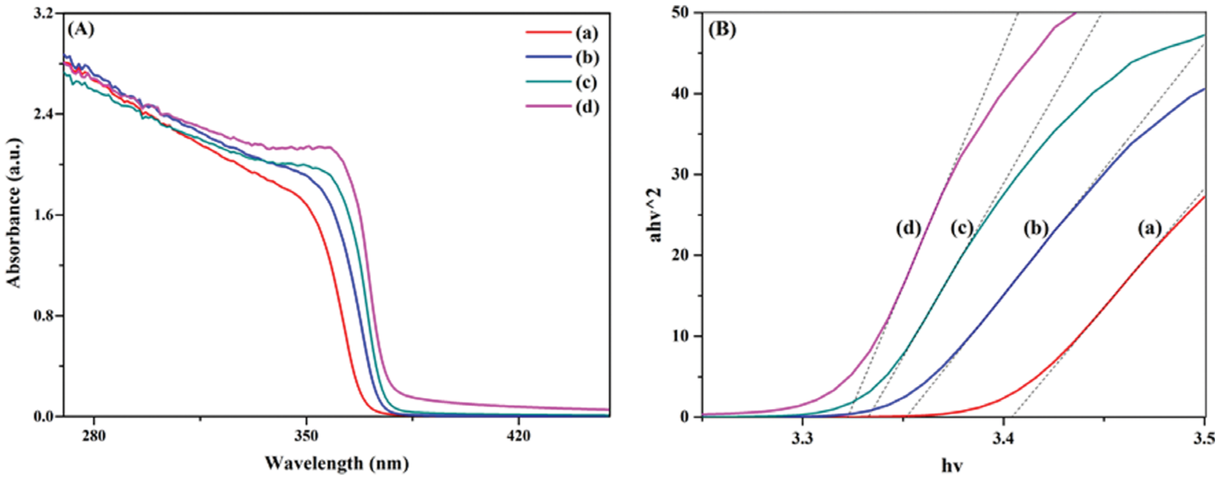

Fig. 5. (A) UV adsorption spectra of ZnO nanoparticles. (B) Tauc plot of $(\alpha hv)^2$ versus photon energy hv of the ZnO samples. (a) ZnO NS, (b) ZnO NR1, (c) ZnO NR3, and (d) ZnO NR5.

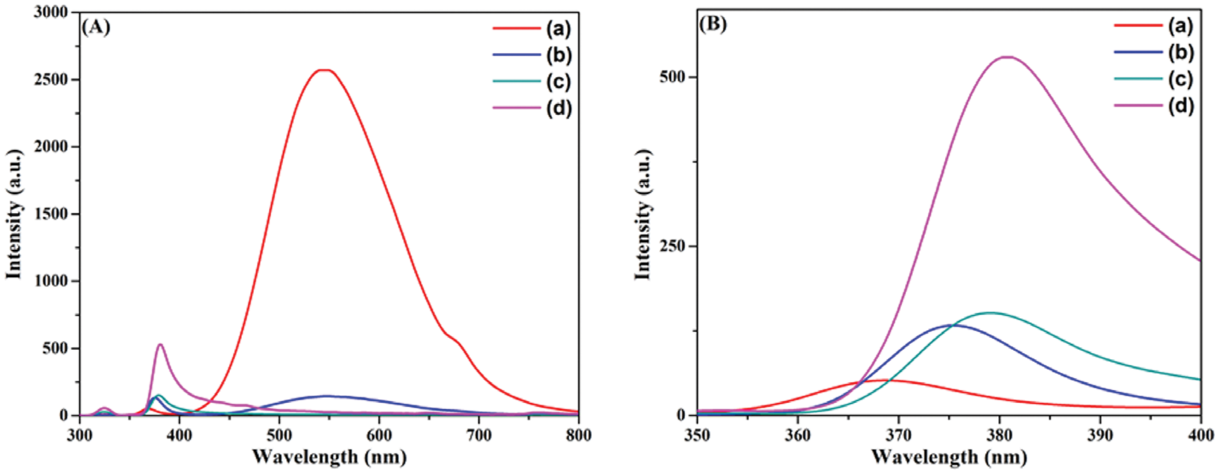

Fig. 6. (A) Photoluminescence spectra of ZnO nanoparticles formed on the different amount of the water from 300 nm to 800 nm located in UV and visible region. (B) from 350 nm to 400 nm located in UV region. (a) ZnO NS, (b) ZnO NR1, (c) ZnO NR3, and (d) ZnO NR5.

Table 3. Intensity details of PL spectra of the ZnO nanosphere and nanorods. (a) ZnO NS, (b) ZnO NR1, (c) ZnO NR3, and (d) ZnO NR5

Sample	NBE peak intensity	DL peak intensity	Intensity ratio $[(I_{NBE})/(I_{DL})]$
(a)	51.7	2570.7	0.02
(b)	132.8	144.6	0.92
(c)	151.5	8.6	17.62
(d)	529	26.2	20.2

emission and the DL emission are related to the radiative recombination of free excitons throughout an exciton-exciton collision process [41] and the recombination of photogenerated electrons and holes with single ionized oxygen vacancies and zinc interstitials [42], which are surface defects in the ZnO particles [43]. In Fig. 6(B), the shift of the NBE emission peak from 368 nm to 381 nm demonstrates the morphological change from spheres to rods due to lowering of the exciton energy [44]. After adding water, it was observed that the DL emission peak disappeared for all of the samples, while the ZnO NS sample exhibited a DL emission peak, indicating an increase of oxygen vacancies as the shape changed to rods. Oxygen vacancies and zinc interstitials act as electron acceptors in the photocatalytic process and temporarily capture photogenerated electrons to hamper the recombination of electrons and holes [45]. Simultaneously, the NBE/DL intensity ratio sharply increased from 0.02 to 20.2, as shown in Table 3. This indicates that the reduction of photogenerated electron and hole recombination facilitates charge separation [46]. Thus, the oxygen vacancies and zinc interstitials can greatly influence the photocatalytic efficiency.

3. Photocatalytic Activity Performance

A photocatalytic reaction mechanism on ZnO nanoparticles in an alkaline solution proposed previously can be described as the following steps [47].

$$\mathrm{ZnO+hv\ (>3.4\ eV)\rightarrow ZnO\ (e^-_{CB}+h^+_{VB})} \tag{1}$$

$$\mathrm{ZnO\ (h^+_{VB})+H_2O_{(ads)}\rightarrow ZnO+OH^{\bullet}+H^+} \tag{2}$$

$$\mathrm{ZnO\ (e^-_{CB})+O_{2(ads)}\rightarrow ZnO+O_2^{\bullet-}} \tag{3}$$

$$\mathrm{H^+ + O_2^{\bullet-}\rightarrow HO_2^{\bullet}} \tag{4}$$

$$\mathrm{OH^{\bullet}\ (or\ HO_2^{\bullet})+MB\ (pollutants)\rightarrow CO_2+H_2O} \tag{5}$$

When the ZnO suspension is irradiated by UV light with a photonic energy (hv) greater than 3.4 eV, an electron from the valence band (VB) is raised to an empty conduction band (CB) and thus produces an electron-hole pair (Eq. (1)). The hydroxy radical ($OH^{\bullet}$) and superoxide radical anion ($O_2^{\bullet-}$) can be generated by redox reactions (Eq. (2) and Eq. (3)). The generated superoxide radical anion ($O_2^{\bullet-}$) reacts with H^+ in water and produces the hydrogen peroxide radical ($HO_2^{\bullet}$) (Eq. (4)). The resulting $OH^{\bullet}$ (or $HO_2^{\bullet}$) oxidizing agents will strike the pollutants adsorbed on the surface of ZnO. The pollutants will then be converted to ecofriendly compounds such as CO_2 and H_2O (Eq. (5)). The photocatalytic properties of the ZnO nanorods were evaluated for the photodegradation of an organic pollutant using an MB aqueous solution. Fig. 7 shows the absorbance spectra of ZnO NS and ZnO NR5 recorded from 500 nm to 750 nm, where the strong absorption band at 664 nm represents the maximum wavelength for methylene blue (MB) dye. Fig. 7 shows that for ZnO NS, the dye was completely photodegraded in 40 minutes, whereas for ZnO NR5, the dye was fully photo-decomposed in ten minutes. Fig. 8(A) indicates that the ZnO NRs obtained with a small amount of water exhibited enhanced photocatalytic decomposition of MB dyes compared to the ZnO NS. The larger photocatalytic activity is due to the aspect ratio and potential difference. As the aspect ratio of 1-D ZnO nanostructures increases, the potential difference between the Zn-rich (001) and O-rich ($00\bar{1}$) surfaces increases due to the formation of alternating layers. Therefore, each surface polarized with positive and negative charges attracts organic pollutants due to electrostatic attractive forces in the aqueous MB solution [48]. As a result, ZnO NR5 displayed the highest photocatalytic efficiency (99.3% photodegradation for 10 min of irradiation), and the lowest photocatalytic efficiency was observed with ZnO NS (49.2% photodegradation for 10 min of irradiation). It could be inferred that the photocatalytic efficiency was influenced by the morphological change of ZnO. The photodegradation process of MB on ZnO nanoparticles obeyed the pseudo-first-order kinetics model. The kinetic models for the

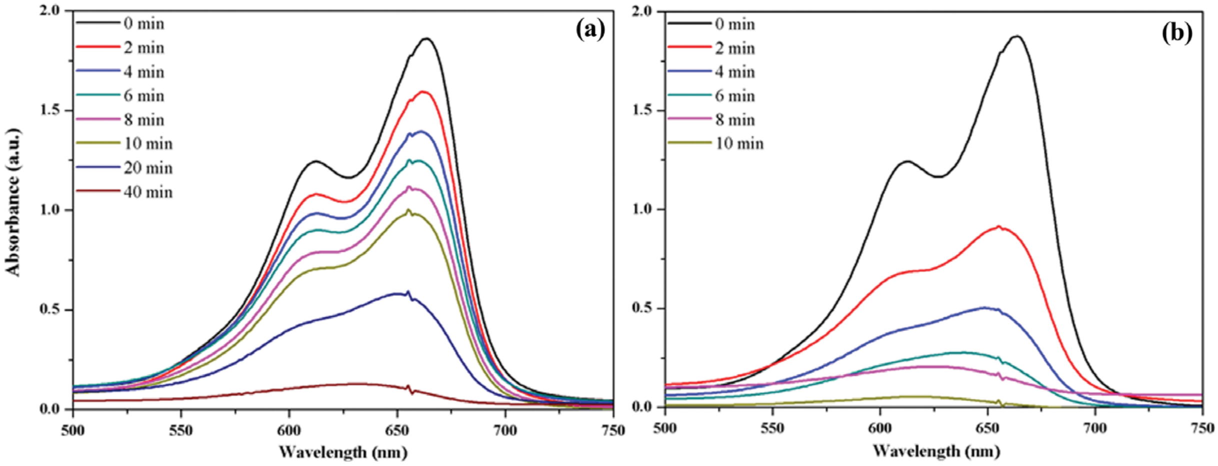

Fig. 7. Photocatalytic degradation of methylene blue (MB) (A) ZnO NS, and (B) ZnO NR5.

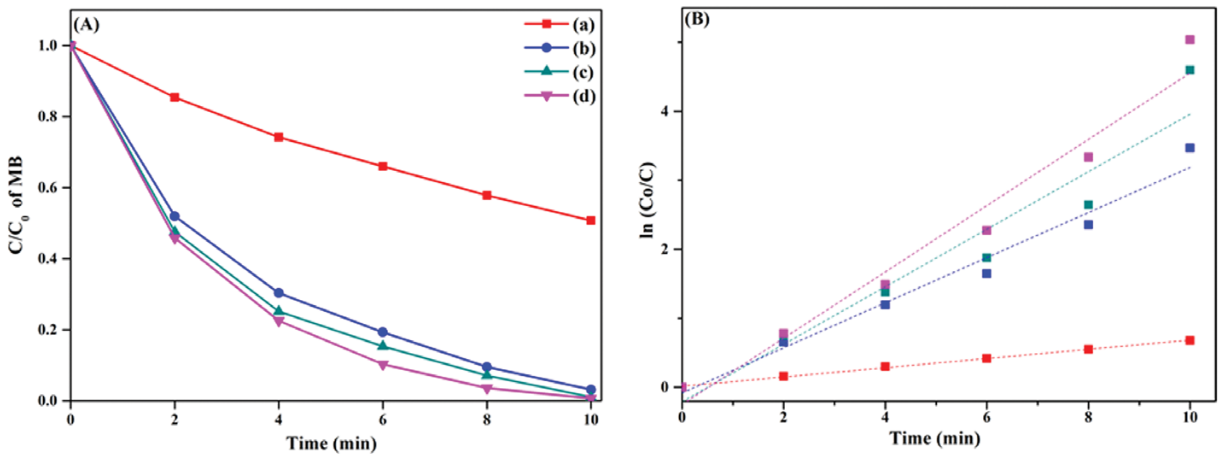

Fig. 8. (A) Photocatalytic degradation for methylene blue (MB) over ZnO nanoparticles and (B) the pseudo-first-order kinetic plot under UV-visible light irradiation (a) ZnO NS, (b) ZnO NR1, (c) ZnO NR3, and (d) ZnO NR5.

degradation of MB can be expressed as follows [49,50]:

$$\ln\frac{C}{C_0}=kt \tag{6}$$

Here, C (mg/L) is the concentration of MB at time t (min) during the reaction, C_0 (mg/L) is the initial concentration of MB, and k is the pseudo-first-order rate constant (min^{-1}). Furthermore, linear graphs of ln(C/C_0) versus the UV irradiation time t (min) are shown in Fig. 8(B). The pseudo-first-order rate constants of ZnO NS and NRs (NR1, NR3, NR5) were measured to be 0.067 min^{-1}, 0.327 min^{-1}, 0.417 min^{-1}, and 0.481 min^{-1}, respectively. The reaction rate constant of ZnO NR5 (k=0.481 min^{-1}) was about seven-times higher compared to ZnO NS (k=0.067 min^{-1}). The results in Fig. 8 demonstrate that the increment of the photocatalytic efficiency was due to the change of morphology. The increase of the number of partial positive and negative charges of Zn (001) and O $(00\bar{1})$ formed by the dangling bonds on the terminated surface of ZnO has a positive impact on the adsorption capacities of H_2O and O_2 on the surface of ZnO [51]. Therefore, accretion of the surface electric charge density increases the capturing of pollutant materials. The surface electric charge density not only facilitates the charge separation and transfer, but also deteriorates the electron-hole recombination [52].

CONCLUSIONS

1D ZnO nanostructures were synthesized by adding water during the sol-gel process. To alter the morphological change of ZnO with C-axis growth, nuclear growth of ZnO particles was performed and the length between the Zn-rich surface (001) and oxygen-rich $(00\bar{1})$ surface was controlled by changing the amount of water. XRD analysis showed that the (002) peak intensity increment was about two-times greater than the (100) increment. The lengths of the ZnO nanorods (NR1, NR3, NR5) were 13 nm, 48.6 nm, and 72.5 nm, respectively. The aspect ratios of the 1-D ZnO nanostructures were 2, 6.6, and 9.7, respectively. The UV-vis spectra of ZnO solutions exhibited a small red shift, which indicates an increase in ZnO nanostructure size and photo-generated carriers. The MB photodegradation capability of ZnO NS was lower than that of the ZnO NRs. Better photocatalytic performance was obtained from ZnO nanorods with a higher aspect ratio. In detail, the photocatalytic efficiency was in the following order: ZnO NR5> ZnO NR3>ZnO NR1>ZnO NS. These results indicate that the improvement of the separation of electron-hole pair in ZnO nanorods can induce more adsorption of H_2O and O_2. The results of this research can be applied for the effective photodegradation of organic pollutants by ZnO particles, including waste water treatment.

ACKNOWLEDGEMENTS

This research was supported by the Basic Science Research Program through the National Research Foundation of Korea (NRF) funded by the Ministry of Education (2016R1A6A1A 03013422).

REFERENCES

1. J. Wang, R. Chen, Y. Xia, G. Wang, H. Zhao, L. Xiang and S. Komarneni, *Ceram. Int.*, **43**, 1870 (2017).
2. J. Mishra, M. Jha, N. Kaur and A. K. Ganguli, *Mater. Res. Bull.*, **102**, 311 (2018).
3. S. G. Kumar and L. G. Devi, *J. Phys. Chem. A*, **115**, 13211 (2011).
4. C. J. Chang, M. H. Hsu, Y. C. Weng, C. Y. Tsay and C. K. Lin, *Thin Solid Films*, **528**, 167 (2013).
5. T. Di, B. Zhu, J. Zhang, B. Cheng and J. Yu, *Appl. Surf. Sci.*, **389**, 775 (2016).
6. L. Mao, H. Liu, S. Liu, Q. Ba, H. Wang, L. Gao, X. Li, C. Huang and W. Chen, *Mater. Res. Bull.*, **93**, 9 (2017).
7. M. R. D. Khaki, M. S. Shafeeyan, A. A. A. Raman and W. M. A. W. Daud, *J. Environ. Manage.*, **198**, 78 (2017).
8. R. Singh, K. Verma, A. Patyal, I. Sharma, P. B. Barman and D. Sharma, *Solid State Sci.*, **89**, 1 (2019).
9. E. Hong, T. Choi and J. H. Kim, *Korean J. Chem. Eng.*, **32**, 424 (2015).
10. B. Weng, M. Q. Yang, N. Zhang and Y. J. Xu, *J. Mater. Chem. A*, **2**, 9380 (2014).
11. R. Raji and K. G. Gopchandran, *J. Phys. Chem. Solids*, **113**, 39 (2018).
12. N. Huang, J. Shu, Z. Wang, M. Chen, C. Ren and W. Zhang, *J.*

Alloys. Compd., **648**, 919 (2015).
13. X. Zhang, J. Qin, Y. Xue, P. Yu, B. Zhang, L. Wang and R. Liu, *Sci. Rep.*, **4**, 4596 (2014).
14. Z. Liu, Z. G. Zhao and M. Miyauchi, *J. Phys. Chem. C*, **113**, 17132 (2009).
15. S. Kato, Y. Hirano, M. Iwata, T. Sano, K. Takeuchi and S. Matsuzawa, *Appl. Catal. B-Environ.*, **57**, 109 (2005).
16. J. Zhang, L. Sun, H. Pan, C. Liao and C. Yan, *New J. Chem.*, **26**, 33 (2002).
17. P. X. Gao and Z. L. Wang, *J. Phys. Chem. B*, **108**, 7534 (2004).
18. J. J. Wu and S. C. Liu, *Adv. Mater.*, **14**, 215 (2002).
19. R. Liu, A. A. Vertegel, E. W. Bohannan, T. A. Sorenson and J. A. Switzer, *Chem. Mater.*, **13**, 508 (2001).
20. Y. W. Heo, V. Varadarajan, M. Kaufman, K. Kim, D. P. Norton, F. Ren and P. H. Fleming, *Appl. Phys. Lett.*, **81**, 3046 (2002).
21. H. Cheng-Liang, C. Shoou-Jinn, H. Hui-Chuan, L. Yan-Ru, H. Chorng-Jye, T. Yung-Kuan and I. Chen, *IEEE T. Nanotechnology*, **4**, 649 (2005).
22. S. Yan, L. Wan, Z. Li and Z. Zou, *Chem. Commun.*, **47**, 5632 (2011).
23. Q. Jijun, L. Xiaomin, H. Weizhen, S. J. Park, H. K. Kim, Y. H. Han, J. H. Lee and Y. D. Kim, *Nanotechnology*, **20**, 155603 (2009).
24. P. Banerjee, S. Chakrabarti, S. Maitra and B. K. Dutta, *Ultrason. Sonochem.*, **19**, 85 (2012).
25. Y. Jeong, J. Y. Kang, I. Kim, H. Jeong, J. K. Park, J. H. Park and J. C. Jung, *Korean J. Chem. Eng.*, **33**, 114 (2016).
26. B. Cheng, W. Shi, J. M. Russell-Tanner, L. Zhang and E. T. Samulski, *Inorg. Chem.*, **45**, 1208 (2006).
27. H. J. Jung, S. Lee, H. C. Choi and M. Y. Choi, *Solid State Sci.*, **21**, 26 (2013).
28. H. Wang, C. Xie and D. Zeng, *J. Cryst. Growth*, **277**, 372 (2005).
29. Y. Chen, H. Zhao, B. Liu and H. Yang, *Appl. Catal. B-Environ.*, **163**, 189 (2015).
30. C. K. Frederik, T. Yi, T. Ralf and W. A. Jens, *Nanotechnology*, **19**, 424013 (2008).
31. J. Boucle, H. J. Snaith and N. C. Greenham, *J. Phys. Chem. C*, **114**, 3664 (2010).
32. J. Q. Hu, Q. Li, N. B. Wong, C. S. Lee and S. T. Lee, *Chem. Mater.*, **14**, 1216 (2002).
33. S. Kundu, S. Sain, B. Satpati, S. R. Bhattacharyya and S. K. Pradhan, *RSC Adv.*, **5**, 23101 (2015).
34. A. McLaren, T. Valdes-Solis, G. Li and S. C. Tsang, *J. Am. Chem. Soc.*, **131**, 12540 (2009).
35. H. Çolak, E. Karaköse and G. Kartopu, *J. Mater. Sci-Mater. El.*, **29**, 11964 (2018).
36. L. Yanhong, W. Dejun, Z. Qidong, Y. Min and Z. Qinglin, *J. Phys. Chem. B*, **108**, 3202 (2004).
37. Z. L. S. Seow, A. S. W. Wong, V. Thavasi, R. Jose, S. Ramakrishna and G. W. Ho, *Nanotechnology*, **20**, 045604 (2008).
38. M. S. Mohajerani, A. Lak and A. Simchi, *J. Alloys. Compd.*, **485**, 616 (2009).
39. T. M. Shang, J. H. Sun, Q. F. Zhou and M. Y. Guan, *Cryst. Res. Technol.*, **42**, 1002 (2007).
40. L. Yang, P. W. May, L. Yin and T. B. Scott, *Nanotechnology*, **18**, 215602 (2007).
41. J. Sun, J. Bian, H. Liang, J. Zhao, L. Hu, Z. Zhao, W. Liu and G. Du, *Appl. Surf. Sci.*, **253**, 5161 (2007).
42. Y. Liu, X. Yan, Z. Kang, Y. Li, Y. Shen, Y. Sun, L. Wang and Y. Zhang, *Sci. Rep.*, **6**, 29907 (2016).
43. K. Choi, T. Kang and S. G. Oh, *Mater. Lett.*, **75**, 240 (2012).
44. Q. Li, J. Bian, J. Sun, J. Wang, Y. Luo, K. Sun and D. Yu, *Appl. Surf. Sci.*, **256**, 1698 (2010).
45. J. Gupta, K. C. Barick and D. Bahadur, *J. Alloys. Compd.*, **509**, 6725 (2011).
46. J. Rouhi, M. Alimanesh, R. Dalvand, C. H. R. Ooi, S. Mahmud and M. R. Mahmood, *Ceram. Int.*, **40**, 11193 (2014).
47. S. A. Vanalakar, S. S. Mali, M. P. Suryawanshi, N. L. Tarwal, P. R. Jadhav, G. L. Agawane, K. V. Gurav, A. S. Kamble, S. W. Shin, A. V. Moholkar, J. Y. Kim, J. H. Kim and P. S. Patil, *Opt. Mater.*, **37**, 766 (2014).
48. C. B. Ong, L. Y. Ng and A. W. Mohammad, *Renew. Sustain. Energy Rev.*, **81**, 536 (2018).
49. G. He, B. Huang, Z. Lin, W. Yang, Q. He and L. Li, *Crystals*, **8**, 152 (2018).
50. X. Chen, Z. Wu, D. Liu and Z. Gao, *Nanoscale Res. Lett.*, **12**, 143 (2017).
51. L. Y. Yang, S. Y. Dong, J. H. Sun, J. L. Feng, Q. H. Wu and S. P. Sun, *J. Hazard. Mater.*, **179**, 438 (2010).
52. Y. Zheng, L. Zheng, Y. Zhan, X. Lin, Q. Zheng and K. Wei, *Inorg. Chem.*, **46**, 6980 (2007).
53. A. Leelavathi, G. Madras and N. Ravishankar, *Phys. Chem. Chem. Phys.*, **15**, 10795 (2013).